ANNUAL REVIEWS

Annual Review of Marine Science

Novel Insights into Marine Iron Biogeochemistry from Iron Isotopes

Jessica N. Fitzsimmons[1] and Tim M. Conway[2]

[1]Department of Oceanography, Texas A&M University, College Station, Texas, USA; email: jessfitz@tamu.edu

[2]College of Marine Science, University of South Florida, St. Petersburg, Florida, USA; email: tmconway@usf.edu

Annu. Rev. Mar. Sci. 2023. 15:383–406

First published as a Review in Advance on September 13, 2022

The *Annual Review of Marine Science* is online at marine.annualreviews.org

https://doi.org/10.1146/annurev-marine-032822-103431

Keywords

iron isotopes, dust, sediments, hydrothermal vents, GEOTRACES, ocean biogeochemistry

Abstract

The micronutrient iron plays a major role in setting the magnitude and distribution of primary production across the global ocean. As such, an understanding of the sources, sinks, and internal cycling processes that drive the oceanic distribution of iron is key to unlocking iron's role in the global carbon cycle and climate, both today and in the geologic past. Iron isotopic analyses of seawater have emerged as a transformative tool for diagnosing iron sources to the ocean and tracing biogeochemical processes. In this review, we summarize the end-member isotope signatures of different iron source fluxes and highlight the novel insights into iron provenance gained using this tracer. We also review ways in which iron isotope fractionation might be used to understand internal oceanic cycling of iron, including speciation changes, biological uptake, and particle scavenging. We conclude with an overview of future research needed to expand the utilization of this cutting-edge tracer.

1. INTRODUCTION

Iron (Fe) is a key micronutrient in the oceans that is required by phytoplankton for photosynthesis, respiration, and nitrogen fixation (Twining & Baines 2013). Although it is the fourth most abundant element in Earth's upper continental crust (Rudnick & Gao 2014), it suffers from extremely low solubility in oxic seawater (Liu & Millero 2002). Consequently, subnanomolar surface-ocean dissolved Fe (dFe) concentrations limit primary production across up to 40% of the global surface ocean (Moore et al. 2002), principally in the high-nutrient, low-chlorophyll Southern, equatorial Pacific, and subarctic Pacific Oceans. Thus, dFe distributions play a major role in controlling global primary production and carbon export (Tagliabue et al. 2017), both in the modern ocean and in the geologic past (Martin 1990).

The climate interest in Fe has sparked a major effort over the last 30 years to learn what controls the global oceanic Fe cycle. The International GEOTRACES Program, which seeks to understand the sources, sinks, and internal cycling of trace elements and their isotopes across ocean sections, has significantly furthered these efforts (Anderson 2020). While the Fe supply was once thought to be dominated by dust fluxes, GEOTRACES has shown that margin sediment and hydrothermal vents may be equally or more significant sources of Fe to the global ocean (reviewed in Tagliabue et al. 2017), while sources such as rivers, glaciers, and sea ice can also be regionally important.

However, marine Fe distributions are more complicated than simple proximity to source. Fe has two oxidation states—the more soluble Fe(II) and the less soluble Fe(III)—and exhibits strong redox sensitivity to pH, oxygen, and photochemical conditions. As a result of these redox transformations, Fe has complex chemical speciation in seawater, with Fe(II) rapidly oxidized to Fe(III) in the presence of oxygen over a timescale of seconds to hours and quickly forming Fe(III) oxyhydroxide precipitates (Liu & Millero 2002). Moreover, the distributions of dFe in the ocean are bolstered above solubility limits by the chelation of Fe by organic ligands, including but not limited to bacterially produced siderophores, terrestrially derived humic acids, and other less specific biological by-products (Gledhill & Buck 2012). These Fe–organic complexes keep Fe dissolved in seawater, as it would otherwise be rapidly scavenged onto sinking particles; instead, the ligand-bound Fe dissolved in seawater is thought to have a residence time of 25–270 years (Bergquist & Boyle 2006a, Hayes et al. 2015).

The complex physicochemical speciation of Fe in seawater means that the Fe pool is operationally defined. For example, total Fe (Fe_T) in seawater is defined as:

$$Fe_T = dFe + pFe = sFe + cFe + pFe,$$

where dFe and particulate Fe (pFe) are operationally separated with a 0.2- or 0.4-μm filter. dFe comprises both soluble Fe (sFe) species, which are truly dissolved Fe compounds (defined as <0.003 μm or <0.02 μm), and colloidal Fe (cFe) species, which are the nanoparticulate Fe species that pass through bulk particle filters but are not truly dissolved (Fitzsimmons & Boyle 2014). sFe, cFe, and pFe species can be organic or inorganic in nature. GEOTRACES has now provided a large database of these Fe concentrations across much of the oceans (Schlitzer et al. 2018).

Fe's complex speciation and range of biotic and abiotic transformations control its oceanic distribution over short timescales (significantly shorter than ocean overturning), allowing for significant regional variability in processes, distributions, and availability to phytoplankton. Such variability has led naturally to efforts to identify and even quantify Fe fluxes to different source regions. GEOTRACES has addressed this effort by comparing Fe distributions with those of chemical tracers unique to individual source fluxes (Anderson 2020). Global Fe biogeochemical modeling efforts have also increased in recent years, and while many of these models emulate observed dFe distributions fairly well, the complexities in parameterizing Fe fluxes and

transformations have led to significant variability in estimates of the magnitude of specific Fe sources and the resulting Fe residence times (Tagliabue et al. 2016).

One additional tool developed in the last 20 years that has revolutionized our ability to identify the sources of Fe to seawater is the measurement of the ratio of the stable isotopes of dFe in seawater. Fe has four natural stable isotopes of varying abundances (^{54}Fe, 5.8%; ^{56}Fe, 91.7%; ^{57}Fe, 2.2%; and ^{58}Fe, 0.3%) and undergoes mass-dependent isotope fractionation (Johnson et al. 2020). The Fe isotope ratio is typically defined as the ^{56}Fe/^{54}Fe ratio expressed in delta notation relative to Institute for Reference Materials and Measurements Standard 014 (IRMM-014) as

$$\delta^{56}\mathrm{Fe} = \left(\frac{^{56}\mathrm{Fe}/^{54}\mathrm{Fe}_{\mathrm{sample}}}{^{56}\mathrm{Fe}/^{54}\mathrm{Fe}_{\mathrm{IRMM\text{-}014}}} - 1 \right) \times 1{,}000 \text{ (in ‰)}.$$

The δ^{56}Fe of upper continental crust material is +0.09‰ (Beard et al. 2003); δ^{56}Fe less than this is said to be isotopically light (containing relatively more of the light isotope ^{54}Fe than the crust), and δ^{56}Fe larger than this is said to be isotopically heavy (containing relatively more of the heavy isotope ^{56}Fe than the crust).

There has been a significant expansion in δ^{56}Fe measurements of seawater in the last 15 years (**Figure 1**), leading to major advances in the diagnosis of Fe sources and internal cycling processes that drive oceanic Fe biogeochemistry. These studies have further stimulated efforts to use δ^{56}Fe in oceanic archives as proxies for redox cycling, source characterization, and paleoproductivity in the past oceans (see the sidebar titled Back Through Time). Here, we review the literature on dissolved δ^{56}Fe in seawater, with an emphasis on how δ^{56}Fe measurements have revolutionized our understanding of marine Fe biogeochemistry. In Section 2, we briefly review Fe isotope methodology and the major Fe isotope fractionation pathways. In Section 3, we characterize the δ^{56}Fe signatures of individual Fe source fluxes to the ocean and their uncertainties, and in Section 4, we highlight several groundbreaking case studies that applied these δ^{56}Fe signatures to quantify

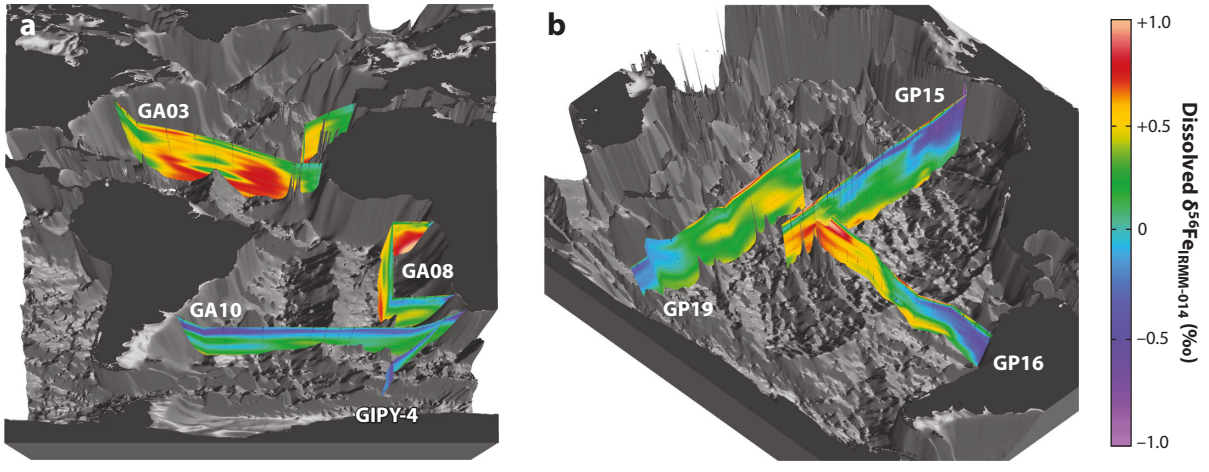

Figure 1

Three-dimensional visualization of dissolved Fe isotope ratios (δ^{56}Fe) along GEOTRACES sections in (*a*) the Atlantic and (*b*) the Pacific. Data are originally from Cyril Abadie, Tim Conway, Jessica Fitzsimmons, Joshua Helgoe, Hannah Hunt, Seth John, François Lacan, Nathan Lanning, Franck Poitrasson, Amadine Radic, Matthias Sieber, Yoshiki Sohrin, Brent Summers, Shotaro Takano, Emily Townsend, and Derek Vance; they are available in the GEOTRACES Intermediate Data Product 2021 (GEOTRACES Int. Data Prod. Group 2021) or are unpublished (GA08 and GP15, provided by Jessica Fitzsimmons and Tim Conway). The visualizations were created and provided by Reiner Schlitzer, Alfred Wegener Institute, Bremerhaven, Germany. Abbreviation: IRMM-014, Institute for Reference Materials and Measurements Standard 014.

BACK THROUGH TIME

δ^{56}Fe measurements have also found utility in studies of the marine Fe cycle in the past. For example, marine ferromanganese crust δ^{56}Fe records have been used to reconstruct oceanic Fe sources back through the Cenozoic to the Cretaceous (Chu et al. 2006, Horner et al. 2015, Levasseur et al. 2004, Marcus et al. 2015, Zhu et al. 2000). Deep marine clays are also emerging as a useful archive for reconstructing the marine Fe cycle (Dunlea et al. 2021), and Fe isotopes have informed our understanding of Cretaceous ocean anoxic events (Owens et al. 2012). While δ^{56}Fe measurements are useful for reconstructing some aspects of the past ocean Fe cycle, recent assessments suggest that they are unlikely to be useful tracers of past ocean productivity (Horner et al. 2021). Back through deep time, Fe isotopes from rock archives have been extensively utilized as proxies for understanding processes such as weathering, global oxygenation, biological activity, and redox cycling in the Precambrian oceans (Johnson et al. 2020).

which Fe sources supply Fe to seawater. In Section 5, we highlight how δ^{56}Fe can also provide insights into the internal cycling of marine dFe under certain conditions, and we conclude in Section 6 with an outlook on what future work is needed to expand the utility of Fe isotopes as a marine biogeochemical tracer.

2. IRON ISOTOPES BACKGROUND: METHODS AND FRACTIONATION PATHWAYS

Measurements of the stable isotope ratio of Fe were first attempted in the mid-1900s using thermal ionization mass spectrometry to analyze terrestrial and extraterrestrial samples (Nier 1939, Valley & Anderson 1947). However, the use of this technique for δ^{56}Fe measurements is challenging for two reasons: (*a*) Fe has a poor thermal ionization efficiency, and (*b*) it suffers from a temporally variable mass bias during vaporization (Beard & Johnson 1999). Thus, when multicollector inductively coupled plasma mass spectrometry (MC-ICP-MS) methods were popularized in the early 2000s, Fe isotope analyses shifted almost entirely to this new analytical platform, where Fe is much more easily ionized, enjoys a more stable mass bias, and benefits from higher sample throughput.

Prior to Fe isotope analysis by MC-ICP-MS, matrix removal of interfering elements is required; wet chemistry methods for Fe purification and strategies for overcoming the molecular argon interferences (e.g., $^{40}Ar^{16}O$ on ^{56}Fe) that plague MC-ICP-MS δ^{56}Fe analyses have been reviewed previously (Johnson et al. 2020). Studies using these methods have shown that δ^{56}Fe in natural terrestrial systems varies by a total of ~8‰, from −4‰ to +4‰, with the majority of the Fe isotope fractionation occurring during low-temperature fluid–mineral reactions (Johnson et al. 2020).

Fe isotope analyses in seawater began in 2007 (de Jong et al. 2007). The seawater matrix introduces extraordinary analytical challenges, including extensive sample processing needed to remove salts to prevent interferences and occlusion of the cone interface in MC-ICP-MS, as well as the rigorous trace metal clean conditions needed to avoid contamination of the low Fe abundances throughout Fe extraction and purification. Additionally, large seawater volumes (1–4 L) are required for δ^{56}Fe analyses in order to concentrate sufficient Fe atoms for a precise measurement, particularly since the three low-abundance Fe isotopes together constitute only 8% of total Fe.

Most seawater Fe isotope methods achieve preconcentration of Fe from the seawater matrix using organic-chelating resins such as nitrilotriacetic acid or Nobias Chelate PA-1 with ethylenediaminetriacetic acid functional groups, followed by anion exchange chromatography to purify

MARINE PARTICLES

Measuring the $\delta^{56}Fe$ in marine particles is challenging, largely due to the variety of particulate Fe mineral structures, which have chemical labilities ranging from refractory to easily exchangeable with the dissolved pool. Strong acid ($HF\text{-}HNO_3$) total digests have been used to dissolve the total particulate pool, while selective chemical leaches are also useful to access the labile, or exchangeable, phase. Here, the major challenge is establishing which leach can access the relevant exchangeable Fe without fractionating the $\delta^{56}Fe$ (Revels et al. 2015b). Despite these challenges, the limited global particulate $\delta^{56}Fe$ data set does provide insights into bio-uptake and scavenging fractionation factors (Ellwood et al. 2015, Labatut et al. 2014, Radic et al. 2011), dFe–pFe cycling and precipitation related to oxygen minimum zones (e.g., Chever et al. 2015, Marsay et al. 2018b, Revels et al. 2015a), nonreductive exchange (Radic et al. 2011), and chemical reactions and transformations (e.g., sulfide versus oxide formation versus ligand exchange) occurring in proximal and distal hydrothermal plumes (e.g., Bennett et al. 2009, Fitzsimmons et al. 2017, Lough et al. 2017, Rouxel et al. 2016, Severmann et al. 2004).

the Fe from isobars using microcolumns to minimize procedural blanks (Conway et al. 2013, John & Adkins 2010, Lacan et al. 2008, Rouxel & Auro 2010). Analysis is then undertaken using the Thermo Scientific Neptune MC-ICP-MS, usually employing special MC-ICP-MS hardware to boost sensitivity (e.g., desolvation introduction systems and high-sensitivity cones) and double spiking techniques to optimize mass bias corrections (Rudge et al. 2009). Suspended pFe filtered from seawater has also been analyzed for Fe isotopes (see the sidebar titled Marine Particles) following bulk digestion of filtered particles (Marsay et al. 2018b, Radic et al. 2011). Partial particulate leaches that mobilize the labile fractions of marine pFe have also been employed but must be used selectively as some leaches cause kinetic isotope fractionation during processing (Revels et al. 2015b).

In aqueous solutions such as seawater, both equilibrium and kinetic isotope effects fractionate Fe isotope ratios during reactions between aqueous components and also between aqueous solutes and solid phases, including minerals (Dauphas et al. 2017). Fe isotope fractionation factors during a chemical reaction are defined as $\Delta^{56}Fe_{product\text{-}reactant} = \delta^{56}Fe_{product} - \delta^{56}Fe_{reactant}$ or as $\alpha_{product/reactant} = (1{,}000 + \delta^{56}Fe_{product}) / (1{,}000 + \delta^{56}Fe_{reactant})$. The primary isotope effect that controls $\delta^{56}Fe$ in low-temperature fluids such as seawater is the equilibrium isotope fractionation between aqueous Fe(II) and Fe(III), with the temperature-dependent equilibrium fractionation factor between the hexaaqua-coordinated species of Fe, $\Delta^{56}Fe_{Fe(III)(aq)\text{-}Fe(II)(aq)}$, being +3.01‰ (Welch et al. 2003), indicating that $Fe(II)_{(aq)}$ should be isotopically lighter by 3‰ than $Fe(III)_{(aq)}$ in equilibrated solutions at 22°C. This redox-dominant equilibrium isotope effect has been corroborated by fractionation experiments between Fe solutes and solid-phase mineral precipitation reactions where, for example, $Fe(II)_{(aq)}$ was precipitated to form hydrous Fe(III)–$ferrihydrite_{(s)}$ with a $\Delta^{56}Fe_{ferrihydrite\text{-}Fe(II)(aq)}$ of +3.2‰ ± 0.2‰ at 25°C (Wu et al. 2011). It is thought that equilibrium Fe isotope fractionation is dominated by the Fe(II)–Fe(III) redox transformation instead of the precipitation to the solid phase, since, for example, the isotopic fractionation between $Fe(III)_{(aq)}$ and $hematite_{(s)}$ is only $\Delta^{56}Fe_{hematite\text{-}Fe(III)(aq)} = -0.1‰ \pm 0.2‰$ at 98°C (Skulan et al. 2002). There are also peculiar differences in equilibrium isotope effects related to specific crystal structures; for example, while the $\Delta^{56}Fe_{ferrihydrite\text{-}Fe(II)(aq)}$ is +3.2‰ ± 0.2‰ at 25°C (Wu et al. 2011), the $\Delta^{56}Fe_{goethite\text{-}Fe(II)(aq)}$ is only +1.05‰ at 25°C (Beard et al. 2010, Frierdich et al. 2014), despite ferrihydrite and goethite being similar Fe oxides. The known equilibrium and kinetic isotope effects associated with the full range of Fe minerals were tabulated and reviewed by Johnson et al. (2020).

The other major equilibrium isotope effect that controls Fe isotope ratios in seawater occurs during the binding of $Fe(III)_{(aq)}$ by organic ligands, which is important since >99.9% of dFe in seawater is thought to be complexed by organic compounds (Gledhill & Buck 2012). Dideriksen et al. (2008) first reported the equilibrium fractionation between hexaaqua-coordinated Fe and that complexed by the strong siderophore desferrioxamine-B (DFOB) as $\Delta^{56}Fe_{DFOB\text{-}hexaaqua\ Fe(III)(aq)} = +0.6‰$ at room temperature. This was expanded to additional Fe-binding organic ligands such as ethylenediaminetetraacetic acid and oxalate (Morgan et al. 2010). A correlation between these organic ligands' $\Delta^{56}Fe_{ligand\text{-}hexaaqua\ Fe(III)(aq)}$ values and their binding affinities (stability constants) shows that equilibrium isotope fractionation favors binding of heavier Fe isotopes by the stronger ligands (Morgan et al. 2010).

3. IRON ISOTOPE END-MEMBER SIGNATURES OF SOURCE FLUXES

Dissolved $\delta^{56}Fe$ in seawater has provided significant insights into which source fluxes supply Fe to the global ocean, with seawater and relevant source materials spanning a large range in $\delta^{56}Fe$ of −5‰ to +2‰ (**Figures 2** and **3**). Fe enters seawater through a variety of pathways, including exchange with sediments, dust solubilization, hydrothermal fluxes, riverine and estuarine fluxes, and cryospheric meltwaters such as glacier and sea ice melt. Each of these source fluxes is variably influenced by Fe isotope-fractionating redox reactions, solid–solute reactions, and ligand stabilization reactions, both in their formation regions (e.g., dust source and subsequent atmospheric processing) and during their introduction into seawater (e.g., dust solubilization in surface waters). Altogether, the isotope effects associated with these cumulative reactions set the $\delta^{56}Fe$ of each Fe

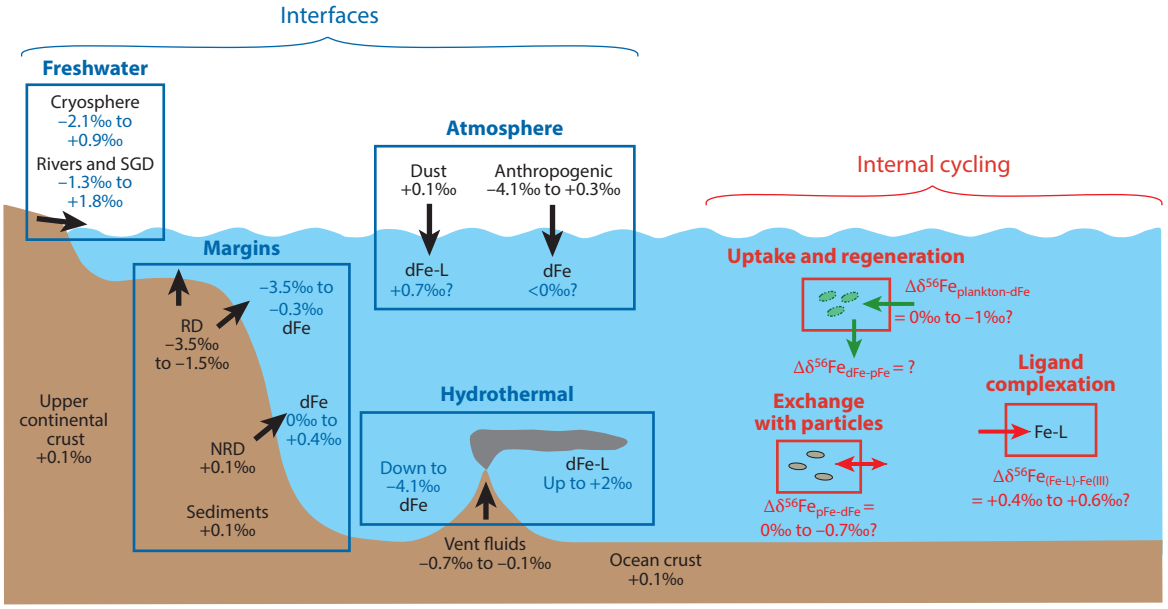

Figure 2

Summary of the Fe isotope source signatures ($\delta^{56}Fe$) and isotope fractionation ($\Delta^{56}Fe$) for internal transformations within the marine Fe cycle. This figure is based on a schematic from the *GEOTRACES Science Plan* (adapted from GEOTRACES Group 2006 with permission from the Scientific Committee on Oceanic Research); citations for the source and fractionation process values can be found in the main text. Abbreviations: dFe, dissolved Fe; L, ligand; NRD, nonreductive Fe dissolution; pFe, particulate Fe; RD, reductive Fe dissolution; SGD, submarine groundwater discharge.

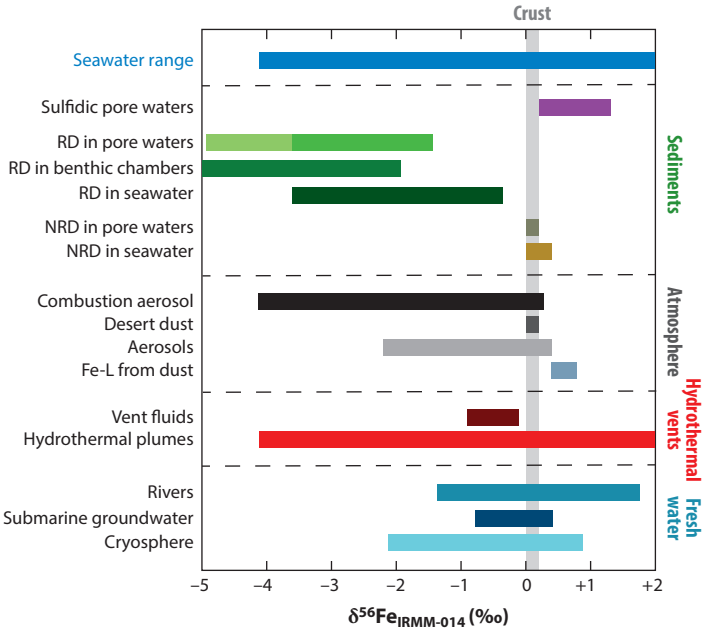

Figure 3

Ranges for Fe isotope end-member signatures (δ^{56}Fe) of major Fe sources to the ocean. For RD in pore waters, darker green indicates dFe produced directly by microbial dissimilatory Fe reduction, and lighter green indicates δ^{56}Fe driven to lighter values by oxidation. Citations for each source can be found in the main text. Abbreviations: dFe, dissolved Fe; IRMM-014, Institute for Reference Materials and Measurements Standard 014; L, ligand; NRD, nonreductive dissolution; RD, reductive dissolution.

source as it enters seawater, resulting in characteristic Fe isotope end-member signatures for each Fe source (**Figures 2** and **3**) that together offer a road map for fingerprinting different sources. However, these signatures do vary regionally, as a function of local conditions. In this section, we review the Fe isotope signatures of each major source flux to the ocean.

3.1. Sediments

Some of the earliest marine Fe isotope studies focused on establishing the Fe isotopic signature of dissolved Fe(II) deriving from microbial dissimilatory Fe reduction (DIR) in sediment pore waters (Bergquist & Boyle 2006b, Homoky et al. 2009, Severmann et al. 2006). DIR—the process of Fe reductive dissolution (RD) associated with anaerobic organic carbon respiration—is considered to be an important Fe release process from sediments into the oceans (Elrod et al. 2004). Pore waters from California margin sediments showed that dissolved Fe(II) formed in situ by RD within the anoxic zone of sediments is isotopically light (δ^{56}Fe from −1.5‰ to −3.5‰), while Fe(II) produced in the sulfidic zone of sediments is isotopically heavier (+0.2‰ to +1.2‰) (Homoky et al. 2013, 2009; Klar et al. 2017a; Roy et al. 2012; Severmann et al. 2006). Production of light Fe(II) during RD is consistent with expectations from laboratory cultures of Fe-reducing bacteria, which show large isotope fractionations (Beard et al. 1999; Crosby et al. 2005, 2007; Icopini et al. 2004; Johnson et al. 2005). dFe formed initially by RD of sediment (δ^{56}Fe of −1.5‰ to −2‰) may then be driven to even lighter values (down to −5‰, but typically ≥−3.5‰) following precipitation of relatively heavy Fe(III) oxyhydroxides, consistent with equilibrium $\Delta^{56}Fe_{Fe(III)(s)\text{-}Fe(II)(aq)}$ (Bullen et al. 2001, Crosby et al. 2007, Homoky et al. 2009, Klar et al. 2017a, Rouxel et al. 2008b, Severmann et al.

2010). The degree of fractionation likely depends on the number of redox cycles in the particular pore water environment (Severmann et al. 2006, 2010).

Once RD was discovered to produce light δ^{56}Fe in pore waters, attention turned to whether such a signature could be transferred to oceanic bottom waters and, if so, serve as a tracer of RD-derived Fe to the ocean interior. The first insights into this question came from benthic chamber incubation and water column studies that showed that isotopically light pore water dFe was transferred to anoxic bottom waters with negligible isotopic fractionation, as seen by signatures of −3.6‰ maintained over 30 incubation hours (Severmann et al. 2010). Persistence of an isotopically light RD signature was also observed in the anoxic bottom waters of the Santa Barbara and San Pedro Basins, with δ^{56}Fe of −3.5‰ and −1.8‰, respectively, averaging −2.4‰ (John et al. 2012b). Estimates of the δ^{56}Fe of the RD benthic Fe flux vary from −0.9‰ to −3.3‰ (summarized in Johnson et al. 2020), driven by variability in local sediment, redox, and water column conditions (Chever et al. 2015; Henkel et al. 2018; Scholz et al. 2014; Severmann et al. 2006, 2010).

Including the above studies, widespread isotopically light Fe (−0.3‰ to −3.6‰) attributed to RD within the oceanic water column has been observed in many near-margin locations across the Atlantic, Pacific, Arctic, and Southern Oceans (Abadie et al. 2017; Chever et al. 2015; Conway & John 2014, 2015; Fitzsimmons et al. 2016; John et al. 2018; Klar et al. 2018; Sieber et al. 2021; Zhang et al. 2021), as well as in restricted partially anoxic basins such as the Baltic and Black Seas (Rolison et al. 2018, Staubwasser et al. 2013). Studies have even suggested that light Fe derived from sediments may be transported over thousands of kilometers through suboxic or oxic ocean waters (John et al. 2018, Sieber et al. 2021). However, over sharp Fe gradients such as those associated with marine oxic–anoxic interfaces, kinetic isotope fractionation during mineral precipitation may be the dominant control on Fe isotope fractionation, instead of equilibrium isotope effects associated with redox transformations, with a reverse fractionation factor inferred within sediments and in several anoxic basins ($\Delta^{56}_{\text{Fe(III)(s)-Fe(II)(aq)}} > 0$‰) (Henkel et al. 2016, 2018; Homoky et al. 2021; John et al. 2012b; Staubwasser et al. 2013). As such, although the proliferation of light Fe through the open ocean suggests that light signatures from RD of marine sediments do survive across oxyclines, further work is needed to distinguish the competing effects of ligand complexation, equilibrium, and kinetic isotope effects in order to best constrain the RD benthic flux end member and how this might vary both with the environment and with the distance away from reductive sources into the ocean interior.

A second mode of sediment dissolution, termed nonreductive dissolution (NRD), was identified based on observations of slightly heavy dFe (+0.4‰) in the water column near Papua New Guinea (Radic et al. 2011), which, although also attributed to sedimentary Fe release, was much heavier than that seen for RD. Further evidence for a mechanism of sedimentary release with only limited fractionation from crustal marine sediments was provided by the observation of near-crustal dFe (+0.2‰ ± 0.2‰) within oxygenated sediment pore waters (Homoky et al. 2009, 2013) and in Fe-rich plumes linked to sedimentary additions in the oxic western North Atlantic (Conway & John 2014) (**Figure 1**). Most recently, it has been suggested that this mode of dissolution, which is also called lithogenic release, occurs by the oxic weathering of sediments to produce colloidal-sized lithogenic particles with crustal δ^{56}Fe (Homoky et al. 2011). The release of Fe from this process is linked to benthic kinetic energy, nepheloid layers, and resuspension events instead of bottom water oxygen (Homoky et al. 2021).

3.2. Dust

Natural aerosol dust and loess have a near-homogeneous Fe isotopic composition (+0.1‰ ± 0.1‰) equivalent to that of the upper continental crust (Beard et al. 2003, Conway et al. 2019, Gong et al. 2017, Mead et al. 2013, Waeles et al. 2007). Furthermore, rapid dissolution of Saharan

aerosol–derived Atlantic aerosols with ultrapure water, seawater, or ammonium acetate solutions shows negligible isotope fractionation of the dFe upon release from dust particles (Conway et al. 2019, Waeles et al. 2007). Together, these lines of evidence suggest that crustal δ^{56}Fe is a good tracer of Fe released by inorganic dissolution of natural aerosol into surface waters, especially in dusty regions of the ocean, such as the North Atlantic (Jickells et al. 2005). However, while suspended pFe from the North Atlantic has a crustal isotope signature (Revels et al. 2015a), dissolved δ^{56}Fe data suggest that the integrated result of dFe released by dust dissolution is, in fact, isotopically heavy (+0.4‰ to +0.8‰), likely as a result of fractionation during organically mediated dust dissolution and internal cycling of Fe within the water column (Conway & John 2014, Fitzsimmons et al. 2015, John & Adkins 2012). As such, using δ^{56}Fe as a simple tracer for atmospheric inputs into the ocean is more complicated than was first hoped.

Using δ^{56}Fe as a surface-ocean dust tracer is further complicated by recent observations that aerosol Fe derived from human sources, such as biomass burning, biofuels, and industrial combustion, can be observed in aerosol dust collected over the ocean (Mead et al. 2013). This anthropogenic Fe is highly soluble and often isotopically light (−4.1‰ to +0.3‰) compared with natural dust and results from biomass burning (Mead et al. 2013) or industrial combustion (Kurisu et al. 2016a,b, 2019; Majestic et al. 2009). These patterns suggest that δ^{56}Fe in aerosols may provide utility in discriminating different sources of aerosol Fe, especially when coupled with dust deposition models (Conway et al. 2019, Kurisu et al. 2021). However, further work is needed to establish the isotopic signatures of these end members—for instance, while Fe released from industrial combustion is reasonably well constrained, biomass-burning Fe signatures are still unknown (although plants are known to be isotopically light; von Blanckenburg et al. 2009). Questions also remain about potential isotopic fractionation of anthropogenic Fe during transport (Mulholland et al. 2021). Furthermore, the isotopic signatures of Fe released by wildfire and volcanic ash emissions are not yet constrained, although fire might be expected to be a mixture of plants and soils (Hamilton et al. 2022, Perron et al. 2022), with the former being light and the latter ranging from −0.2‰ to +0.9‰ (reviewed in Johnson et al. 2020). In sum, while δ^{56}Fe is a promising emerging tracer for distinguishing the different types of Fe in atmospheric aerosols, the isotopic signature of atmospheric Fe (and, more importantly, the soluble Fe fraction) delivered to the surface ocean varies regionally, in addition to any biological fractionation in surface waters (see Section 5.1), precluding a simple δ^{56}Fe end member to the oceans.

3.3. Hydrothermal Vents

Hydrothermal fluids have a range of tectonic histories and subseafloor circulation pathways that result in diverse fluid temperatures and chemical compositions (German & Seyfried 2014). The highest-temperature black smoker fluids are typically acidic and anoxic, and thus they leach Fe as Fe(II) from subsurface rocks up to millimolar concentrations, more than a million times greater than deep-ocean subnanomolar Fe concentrations. The δ^{56}Fe of these high-temperature hydrothermal fluids is not uniform, ranging from −0.69‰ to −0.12‰. However, they are all isotopically light compared with igneous rock sources ($\delta^{56}Fe_{basalt}$ of +0.11‰ ± 0.01‰; Teng et al. 2013), likely due to preferential leaching of isotopically light Fe in the high-temperature subseafloor reaction zone, which leaves the Fe-depleted basalts isotopically heavy (Rouxel et al. 2003). Hydrothermal host rock type affects hydrothermal δ^{56}Fe, as ultramafic (mantle)–hosted hydrothermal fluids have slightly heavier fluid δ^{56}Fe (−0.23‰ ± 0.09‰ and −0.12‰ ± 0.09‰ at two sites on the Mid-Atlantic Ridge) than basalt-hosted fluids (−0.25‰ to −0.7‰) (Beard et al. 2003; Bennett et al. 2009; Nasemann et al. 2018; Rouxel et al. 2008a, 2016; Severmann et al. 2004; Sharma et al. 2001). Additionally, while hydrothermal vapor-brine phase separation appears to fractionate δ^{56}Fe

only mildly (<0.15‰; Beard et al. 2003), the fluid's subseafloor reaction environment can influence δ^{56}Fe much more. For example, one of the heaviest hydrothermal fluids observed to date comes from Loihi Seamount, a low-temperature (<60°C), highly acidic venting system that mixes with seawater in the subseafloor reaction zone, resulting in a δ^{56}Fe of +0.05‰ ± 0.21‰ (Rouxel et al. 2018), indistinguishable from the δ^{56}Fe of its basaltic host.

The largest hydrothermal δ^{56}Fe fractionation occurs in the seawater hydrothermal plume, where hot reducing hydrothermal fluids mix with oxic seawater before reaching neutral buoyancy, at which point they extend horizontally into the abyssal ocean. A multitude of abiotic and biotic Fe transformations move Fe from the dissolved to particulate phase in hydrothermal plumes, such that it was discovered only recently that a small fraction of hydrothermal Fe is in fact stabilized in the dissolved phase and contributes to the oceanic dFe inventory (Fitzsimmons et al. 2014, Resing et al. 2015, Tagliabue et al. 2010). Often the first Fe reaction that occurs in hydrothermal plumes is pyrite formation, which exhibits a kinetic isotope effect of $\Delta^{56}Fe_{pyrite\text{-}dFe} = -0.60‰ \pm 0.12‰$ (Bennett et al. 2009, Butler et al. 2005). This can occur subsurface prior to venting, or upon venting to form the black smoke particles or pyrite nanoparticles that are isotopically light, leaving the remaining Fe(II) isotopically heavier than the vent fluid (Klar et al. 2017b, Lough et al. 2017). Then the oxygen carried by entrained seawater oxidizes the Fe(II) to Fe(III), which is associated with a large +3‰ isotope effect (Welch et al. 2003) and potential additional kinetic isotope effects associated with the subsequent precipitation of Fe (oxyhydr)oxide colloids or particles. These cumulative redox and precipitation reactions drive the remaining dFe to be isotopically light, sometimes as light as −3‰ to −4‰ (Wang et al. 2021), and the precipitated Fe(III) (oxyhydr)oxides to be isotopically heavy, relative to the initial vent fluid.

The other major mechanism of dFe stabilization in the hydrothermal plume is through complexation by organic ligands (Sander & Koschinsky 2011), when strong organic complexes preferentially bind isotopically heavy Fe (Morgan et al. 2010). Consequently, in the distal reaches of aged hydrothermal plumes, where much of the nanoparticulate Fe has aggregated or been removed onto particles (Ellwood et al. 2015), the ligand-bound Fe is thought to be the primary form of persistent hydrothermal dFe (Fitzsimmons et al. 2017), a hypothesis supported by the isotopically heavy δ^{56}Fe of ≥+0.5‰ observed in distal hydrothermal plumes (Fitzsimmons et al. 2016, 2017; Sieber et al. 2021). Thus, altogether, hydrothermal vents can source isotopically light or heavy Fe into seawater (**Figures 2** and **3**), depending on the host rock and fluid geochemistry of the vent, as well as the environmental conditions driving reactions over time within the hydrothermal plume.

3.4. Rivers and Estuaries

Rivers host a wide range of δ^{56}Fe (−1.34‰ to +1.78‰), not because of particularly strong redox gradients but due to the diverse physicochemical speciation that riverine Fe can exhibit. Riverine dFe can be bound to organic ligands of soluble or colloidal size or exist as nanoparticulate clays, Fe (oxyhydr)oxides, or other minerals.

There are three major trends in riverine δ^{56}Fe. First, rivers with high suspended particle loads and low organic content have dissolved δ^{56}Fe indistinguishable from crustal values, consistent with Fe release sans fractionation during physical rock weathering into nanoparticles of similar speciation as riverine particles (Han et al. 2021, Ingri et al. 2006). By contrast, the second river type, with low suspended particle loads but high organic content (e.g., the Negro River and Amazon; Bergquist & Boyle 2006b, Mulholland et al. 2015), has isotopically heavy dissolved δ^{56}Fe (+0.25‰ to +1.78‰), consistent with the mobilization of isotopically heavy Fe bound by organic ligands. This trend is observed in tropical, boreal, and temperate organic-rich rivers (Akerman et al. 2014; Escoube et al. 2009, 2015; Hirst et al. 2020). There has also been a nice demonstration across Fe

size fractions, showing the heaviest δ^{56}Fe in the smallest Fe size fractions, which have low Fe/C ratios, while the more crustal δ^{56}Fe is in the largest colloidal or particulate size fractions, which have the highest Fe/C ratios (Ilina et al. 2013). The third river type has isotopically light dissolved δ^{56}Fe (0‰ to −1.34‰) as a result of Fe supply from organic-rich soil horizons experiencing DIR in the river's watershed (Escoube et al. 2015, Fantle & DePaolo 2004, Han et al. 2021). Light riverine δ^{56}Fe can also derive from anthropogenic Fe inputs in urban or industrialized areas (Chen et al. 2014, Han et al. 2021). Submarine groundwaters are sparsely sampled, but the limited dissolved δ^{56}Fe data that exist show a range from −0.8‰ to +0.4‰ (Rouxel et al. 2008b, Teutsch et al. 2005).

In estuaries, where river water meets seawater, the ionically driven process of flocculation removes a majority of riverine Fe to the estuarine sediments (Boyle et al. 1977). Thus, it was important to establish whether flocculation fractionates δ^{56}Fe in order to understand what the riverine δ^{56}Fe fingerprint is on the ocean. It was hypothesized early on that physical aggregation of Fe and organics should not carry an isotope effect (Beard et al. 2003). However, early experimental simulations of estuarine mixing suggested that flocculation would leave the dissolved δ^{56}Fe isotopically light by up to 1‰ (Bergquist & Boyle 2006b). This was supported by the earliest investigation of natural estuarine δ^{56}Fe (de Jong et al. 2007) and studies of subterranean estuaries (−4.9‰ to +0.4‰; Rouxel et al. 2008b), though in both cases the presence of redox-associated processes complicated the interpretation. However, other field-based investigations have shown no evidence of isotopic fractionation during charge-based flocculation (Escoube et al. 2009), including a conservative δ^{56}Fe budget when the Negro and Solimões tributaries mix into the Amazon with >50% Fe loss (Poitrasson et al. 2014). Thus, wide spatiotemporal variability of riverine δ^{56}Fe is interpreted to result from changes to the physicochemical speciation of its Fe supply, and the freshwater δ^{56}Fe fingerprint is so far thought to be faithfully transferred through the estuary to act on seawater, so long as redox transformations are absent.

3.5. Cryospheric Meltwaters

Fe supply from cryospheric meltwaters (glaciers, sea ice, and snow) has gained attention in recent years as global warming accelerates meltwater production (Lannuzel et al. 2016, Raiswell et al. 2006). The δ^{56}Fe in these cryospheric reservoirs, however, is poorly constrained and widely variable. An early study of bulk Antarctic pack ice found a wide range of dissolved δ^{56}Fe, spanning from −1.5‰ to +0.9‰, with the brine channels showing even lighter dissolved δ^{56}Fe of −1.5‰ to +0.1‰ and particulate δ^{56}Fe of −3.4‰ to −0.2‰ (de Jong et al. 2007); the authors attributed the large variability to biological fractionation within sea ice. A more recent study of Arctic sea ice found a narrower but still broad range of dissolved δ^{56}Fe of −1.10‰ to −0.17‰ (Marsay et al. 2018a). This same study reported dissolved δ^{56}Fe of Arctic snow (−0.38‰ to −0.61‰) and melt ponds (−1.90‰ to +0.13‰) and suggested that photochemical or biological reduction of Fe to isotopically light Fe(II) must be responsible for the light δ^{56}Fe signatures of Arctic snow, sea ice, and melt pond systems.

Fe in glacial melt is similar to that in rivers. In physically weathered Greenland glacial streams, for example, dissolved δ^{56}Fe appears to fall within the crustal array, similar to particulate δ^{56}Fe, regardless of Fe loss during transport (Schroth et al. 2011, Stevenson et al. 2017, Zhang et al. 2015). By contrast, the Fe from subglacial streams can have δ^{56}Fe as isotopically light as −2.1‰ as a result of incongruent silicate weathering and pyrite oxidation (Stevenson et al. 2017). This isotopically light subglacial Fe, in combination with DIR in glacial Fe deposits that leaves pore water δ^{56}Fe isotopically light, has made it more difficult to use δ^{56}Fe in sediment cores to quantify glacial Fe fluxes to Antarctic margins than was initially hoped (Henkel et al. 2018).

4. INSIGHTS INTO MARINE IRON BIOGEOCHEMISTRY GAINED FROM GEOTRACES IRON ISOTOPE SECTIONS

The development of δ^{56}Fe methods for seawater in the late 2000s coincided with the onset of the international GEOTRACES program, which began by undertaking intercomparison exercises in 2008 and 2009 (Anderson et al. 2014). By this time, four laboratories had demonstrated the ability to measure dissolved δ^{56}Fe accurately in seawater at the precision (<0.1‰) required to investigate natural variability, and intercomparison has been excellent across international groups (Boyle et al. 2012, Conway et al. 2016, Ellwood et al. 2020). The outcome of this is that δ^{56}Fe sections and data sets generated by international groups can be interpreted as a single synthesized product (**Figure 1**).

The first pioneering studies to investigate dissolved δ^{56}Fe variability in the oceans recorded a range of >4‰, even in just the first 50 sample analyses (John & Adkins 2012, John et al. 2012b, Radic et al. 2011). Extension of these methods to rapid-throughput analyses (Conway et al. 2013) led to the first ocean section of dissolved δ^{56}Fe (~500 samples; Conway & John 2014). The global δ^{56}Fe data set has continued to grow apace since then. At the time of writing, dissolved δ^{56}Fe data are available for eight full GEOTRACES sections spanning the Atlantic, Pacific, Southern, and Arctic Oceans (GA03, GA08, GA10, GIPY4, GN01, GP15, GP16, and GP19), with the Pacific and Atlantic subsets shown in **Figure 1**. These studies are complemented by a range of smaller-scale process studies, which together with GEOTRACES brings the total marine dissolved δ^{56}Fe data availability to 3,063 data points [tabulated in Conway et al. 2021, which includes data from the GEOTRACES Intermediate Data Product 2021 (GEOTRACES Int. Data Prod. Group 2021), Pinedo-González et al. 2020, Wang et al. 2021, and Zhang et al. 2021 as well as the unpublished GA08 and GP15 data shown in **Figure 1**]. This explosion in seawater δ^{56}Fe data has provided great leaps in our understanding of the marine Fe cycle, including a range of novel insights into the importance of discrete oceanic Fe sources, dFe transport and longevity, and the speciation and form of the dFe pool. Here, we highlight four examples of how Fe isotope studies have driven novel advances in understanding the marine Fe cycle.

4.1. Quantifying the Importance of Multiple Iron Sources

GEOTRACES GA03, the first high-resolution dissolved seawater δ^{56}Fe isotope section in the oceans, spanned the subtropical Atlantic from Europe to the United States via the African Mauritania margin (Conway & John 2014). Given assumptions of the δ^{56}Fe signatures of relevant potential sources to this region (e.g., sedimentary dissolution, dust, and hydrothermal venting), Conway & John (2014) created a simple isotope mass balance model that solved for the fraction that each source contributed to total dFe at each oceanic location:

$$\delta^{56}\mathrm{Fe}_{\mathrm{meas}} = \delta^{56}\mathrm{Fe}_{\mathrm{A}} f_{\mathrm{A}} + \delta^{56}\mathrm{Fe}_{\mathrm{B}} f_{\mathrm{B}},$$

$$f_{\mathrm{A}} + f_{\mathrm{B}} = 1,$$

where f is the fraction of Fe contributed by source A or B. Their quantitative results showed that the subtropical North Atlantic is characterized by point sources ranging from isotopically light to crustal Fe (−1.4‰ to +0.1‰) associated with deep margin sources (sediments and Mid-Atlantic Ridge venting) atop a pervasive background of dust-derived, isotopically heavy dFe (+0.7‰). In fact, isotopically heavy dFe was unexpected prior to this study (see Section 3.2), since characterized oceanic Fe sources were light or crustal, but was attributed to the solubilization of isotopically heavy Fe from dust by organic ligands (Dideriksen et al. 2008, Morgan et al. 2010). The distribution of Fe sources across the GA03 section was fortuitous, as Conway & John (2014) were able to divide the section into regions where only two sources were significant: dust and sediments.

They calculated that 71–87% of the GA03 dFe came from dust, 1–4% from RD in sediments, 2–6% from hydrothermal venting, and 10–19% from NRD in sediments. This was the first study to quantify different Fe sources to an ocean basin, but it also highlights the GEOTRACES consensus that a panoply of deep Fe sources influence the Fe cycle. Perhaps the most notable finding of this study was the inferred importance and proliferation of Fe sourced from NRD on the oxic margin of North America into the western Atlantic, consistent with the developing understanding from pore water studies (Homoky et al. 2013). Quantitative modeling of δ^{56}Fe signatures such as those on GA03 has not been attempted since due to the regional applicability of endmember δ^{56}Fe signatures and potential interferences from internal cycling δ^{56}Fe fractionation (see Section 5). However, the strategy of identifying Fe sources based on δ^{56}Fe signatures is now quite routine and has been used to diagnose multiple specific Fe supply mechanisms that we discuss next.

4.2. Distinguishing Sedimentary Dissolved Iron Supply Mechanisms

Historically, sediment geochemists, biogeochemical modelers, and early pioneers of δ^{56}Fe analyses regarded the main dissolution pathway for Fe in sediments to be DIR under anoxic conditions (Dale et al. 2015, Elrod et al. 2004, Froelich et al. 1979). δ^{56}Fe studies within sediment pore waters, benthic incubation chambers, and the overlying water column in such environments confirmed RD-derived efflux of isotopically light Fe(II) with a signature that persists into bottom waters, highlighting δ^{56}Fe as a promising (local) sediment-derived Fe tracer (Section 3.2). This reductive Fe production mechanism was thought to be important only where organic carbon supply is high, for example, on marginal shelves and under productive upwelling regions. In locations meeting those criteria, δ^{56}Fe has been used to diagnose the presence or absence of RD-derived Fe—for instance, Arctic river-derived water rich in dFe near the North Pole crosses the productive Arctic continental shelves, where RD is expected, but near-crustal δ^{56}Fe confirmed a riverine, not RD, dFe source (Charette et al. 2020, Zhang et al. 2021). Additionally, GEOTRACES sections have confirmed the presence of light dissolved δ^{56}Fe in open ocean waters, indicating that the RD-derived light δ^{56}Fe signature survives oxic conditions and can be traced over thousands of kilometers from the margins, even when concentrations are not especially elevated (John et al. 2018, Sieber et al. 2021) (**Figure 1**).

Moreover, GEOTRACES dissolved δ^{56}Fe studies are responsible for the discovery of the novel NRD pathway in sediments, with its distinctive crustal or slightly heavy signature (Radic et al. 2011). This dissolution mechanism, akin to oxic weathering of sediment, is thought to produce Fe(III) colloids in oxic sediment pore waters that are then released into bottom waters by sediment resuspension (Homoky et al. 2021). Since this mechanism has no dependence on organic carbon flux or benthic oxygen and produces Fe in a form that may persist longer than Fe(II), it may dominate in deeper parts of the ocean (Homoky et al. 2011). In fact, these NRD Fe signals are found globally (**Figure 1**), including in the western North Atlantic (Conway & John 2014), the Pacific (Conway & John 2015, John et al. 2018, Labatut et al. 2014), and the Southern Ocean (Abadie et al. 2017). Prior to dissolved δ^{56}Fe measurements, these deep NRD-derived Fe sources were unknown, whereas now they are beginning to be incorporated into global biogeochemical Fe models (König et al. 2021).

4.3. Distinguishing Anthropogenic and Natural Aerosol Iron

With natural dust aerosol constrained as crustal (+0.1‰; Beard et al. 2003) and the urgent need for a reliable tracer of the presence of anthropogenic Fe within atmospheric aerosols that are delivered to the ocean, the hunt was on to determine whether nonnatural Fe sources such as

industrial combustion might have δ^{56}Fe signatures that were resolvable from desert dust. The first insight came from a time series of aerosol δ^{56}Fe collected on Bermuda (Mead et al. 2013), which showed that although atmospheric particles were dominated by natural dust, isotopically light Fe that might be nonnatural occurred in the winter, when the Saharan dust flux is lower. In two papers from Japan, Kurisu et al. (2016a,b) showed that combustion sources do generate isotopically light aerosol Fe (−4.1‰ to +0.3‰), with the isotopically lightest Fe being present in the smallest particles, which are the ones most likely to persist long distances into the open ocean. Furthermore, they showed that these combustion-derived particles liberate even lighter Fe (down to −4.7‰) when they dissolve in water (Kurisu et al. 2019). Analyses of δ^{56}Fe in bulk and water-soluble aerosols collected on GEOTRACES cruises in both the North Atlantic and the Pacific have similarly revealed light signatures in natural marine aerosols (Conway et al. 2019, Kurisu et al. 2021). In these studies, the authors then applied a two-component isotope mixing approach to both quantify the presence of industrial combustion versus desert dust in aerosols and inform and improve the parameterization of global dust deposition models. Isotopically light Fe has also been observed in surface waters in the North Pacific and been attributed to anthropogenic deposition (Pinedo-González et al. 2020). While work is still underway to best characterize appropriate end members, δ^{56}Fe shows great promise in this area.

4.4. Iron Speciation in Hydrothermal Plumes

While hydrothermal Fe was historically thought to be quantitatively removed to sediments via sinking particles near vent sites, early modeling of hydrothermal Fe suggested that some dFe leaked through to the open ocean (the leaky vent hypothesis) and could fertilize primary production upon upwelling in the Southern Ocean (Tagliabue et al. 2010). In 2014–2015, discovery of the transport of vent-derived dFe over 4,000 km from the southern East Pacific Rise into the abyssal South Pacific shattered any remaining vestiges of earlier paradigms, proving the leaky vent hypothesis (Fitzsimmons et al. 2014, Resing et al. 2015). Since then, ongoing efforts have investigated the mechanisms of dFe stabilization in hydrothermal plumes, including chelation by organic ligands and the stabilization of nanoparticulate sulfides or oxyhydroxides (Gartman et al. 2014, Sander & Koschinsky 2011). Barring analytical methods to distinguish inorganic nanoparticles from organically bound dFe in seawater, δ^{56}Fe has provided critical constraints on dFe physicochemical speciation in hydrothermal plumes. For example, δ^{56}Fe measurements on the US GEOTRACES GP16 South Pacific zonal section showed that the large southern East Pacific Rise plume is sustained by reversible particle–ligand interactions, with the δ^{56}Fe of the plume evolving from mostly nanoparticulate Fe oxyhydroxides in the near field (−0.2‰) to only dissolved ligand complexes in the far field (+0.68‰) as the nanoparticles aggregated away (Fitzsimmons et al. 2017). Closer to the vent sites, measurements and modeling of δ^{56}Fe have provided additional insights into not only Fe speciation but also the oxidation timescales and rates of the Fe transformations that set the dFe concentration that extends into the abyssal ocean (Bennett et al. 2009; Lough et al. 2017; Rouxel et al. 2008a, 2016, 2018; Severmann et al. 2004). Therefore, while the δ^{56}Fe of hydrothermal dFe is variable (**Figure 3**) and thus not diagnostic on its own, combining it with hydrothermal chemical composition (e.g., Fe/H_2S) allows it to provide extremely valuable insights into hydrothermal Fe speciation, reactivity, and fate upon mixing into the global ocean.

5. IRON ISOTOPE FRACTIONATION DURING INTERNAL OCEANIC CYCLING PROCESSES

The application of δ^{56}Fe as an Fe source tracer is quite mature, but in order for this tracer technique to operate, it must be assumed that end-member signatures are set at their sources and

then are not further fractionated by internal cycling processes. While global data sets do support long-distance fidelity of δ^{56}Fe signatures (e.g., carried in Antarctic Intermediate Water; Abadie et al. 2017, Fitzsimmons et al. 2016, Lacan et al. 2008, Sieber et al. 2021), this assumption is not always true, as internal cycling processes (biological uptake, scavenging to particles, oxidative precipitation, and organic complexation) can fractionate source δ^{56}Fe signals and therefore must be considered and constrained. Overall, the role of δ^{56}Fe fractionation during internal cycling Fe transformations has been much less well studied in seawater than in the Fe source regions. We review progress and uncertainties in those fractionation factors here and show that quantifying the Fe isotope fractionation of these different internal cycling processes can also provide us with valuable insight into those specific processes.

5.1. Biological Uptake

An obvious target for internal cycling studies of Fe isotopes is the potential isotope effect during assimilation of Fe by phytoplankton. A priori, we might expect that uptake of Fe into cells would be under kinetic control and as such favor the lighter Fe isotopes, leading to an expressed isotope fractionation, as is seen with the other trace metals (such as cadmium and zinc) in culture (John et al. 2007, Lacan et al. 2006). That said, different phytoplankton acquire specific dFe species using different Fe transport systems, which include direct Fe(II) transporters, cell-surface reductases of Fe(III) to Fe(II), and siderophore-mediated transporters for specific Fe–ligand complexes (discussed in Hutchins et al. 1999, Morel et al. 2008). Since these processes would likely induce different isotope effects, uptake fractionation could add a new dimension to understanding uptake mechanics. However, to date, the challenges of culturing (e.g., Fe precipitation, bottle wall adsorption, and ligand fractionation effects) have so far precluded clear estimates of Fe isotope fractionation of phytoplankton in culture, though efforts are ongoing (John et al. 2012a). Instead, limited insights are provided by a handful of open ocean field studies that compare dissolved and particulate δ^{56}Fe in the euphotic zone. For instance, studies in the equatorial Pacific and the Southern Ocean have suggested that phytoplankton are −0.13‰ to −0.25‰ (Radic et al. 2011) and −0.54‰ (Ellwood et al. 2015) lighter than the dFe pool, respectively. Regeneration of light biogenic material has been invoked to explain the large-scale patterns of light δ^{56}Fe in the South Atlantic (Abadie et al. 2017, König et al. 2021), though this has also been explained as an isotopically light source signal (Sieber et al. 2021).

Most recently, pseudoclosed systems such as the Antarctic Mertz Polynya and a Southern Ocean eddy have been used to demonstrate a preference for light Fe during biological assimilation, with a calculated $\alpha_{cell/dFe}$ fractionation factor of 0.999, which is equivalent to a $\Delta^{56}Fe_{cell\text{-}dFe}$ of approximately −1‰ (Ellwood et al. 2020, Sieber et al. 2021). However, modeling has shown that this $\Delta^{56}Fe_{cell\text{-}dFe}$ can also be explained by a mix of bio-uptake at −0.6‰, regeneration at +0.15‰, scavenging at −0.3‰, and complexation at +0.6‰ (Ellwood et al. 2020), which could explain the large range of $\alpha_{cell/dFe}$ (0.9985 to 0.99985) required to satisfy surface δ^{56}Fe variability across the Southern Ocean (Sieber et al. 2021). While this highlights that more work is needed, it also suggests that the net $\Delta^{56}Fe_{cell\text{-}dFe}$ of biological Fe uptake is likely −0.5‰ to −1‰ ($\alpha_{cell/dFe}$ of 0.999 to 0.9995), which is equivalent to that used in the first attempt to model global Fe isotope distributions (König et al. 2021).

Lastly, it is worth noting that in observations of the euphotic zone prebloom and in the deep chlorophyll maximum of the North Atlantic, net biological activity [e.g., grazing, microbial production of Fe(II), and selective acquisition of Fe species] may actually drive the dFe pool light (Conway & John 2014, Ellwood et al. 2015). Such observations highlight the promise of using process studies to constrain Fe speciation and internal cycling.

5.2. Scavenging and Iron Complexation Effects

A second target for internal Fe cycling studies of Fe isotopes is the potential isotope effect during scavenging of Fe from the dissolved to the particulate phase, as Fe is a hybrid-type element that is both biologically cycled and abiotically scavenged onto sinking particles. The term scavenging includes dFe adsorption onto marine particle surfaces, dFe aggregation or coagulation through colloids to particles, and coprecipitation of dFe during the formation of mineral structures. Fe scavenging can be reversible or irreversible and can be organically or inorganically hosted. Given the variety of Fe species and molecular processes involved in scavenging, it is perhaps no surprise that a single isotope effect for this process has not been assigned.

The earliest experimental investigation of adsorption-based Fe isotope effects observed that $Fe(II)_{(aq)}$ was lost by adsorption onto goethite minerals with a $\Delta^{56}Fe_{adsorbed\text{-}Fe(II)(aq)}$ of +2‰ (Icopini et al. 2004). However, given the potential for redox transformations in that adsorption experiment, their observed fractionation is likely much larger than would be observed in Fe(III)-dominated natural systems such as seawater. Fe isotope effects associated with natural oceanic scavenging were first empirically assigned based on comparisons of dissolved and particulate $\delta^{56}Fe$ outside of the bioactive euphotic zone, with a $\Delta^{56}Fe_{pFe\text{-}dFe}$ of −0.2‰ to −0.3‰ (Radic et al. 2011) and $\Delta^{56}Fe_{pFe\text{-}dFe}$ of −0.27‰ ± 0.25‰ (Labatut et al. 2014). In a hydrothermal plume, this scavenging was observed to have a larger $\Delta^{56}Fe_{pFe\text{-}dFe}$ of −0.67‰ (Ellwood et al. 2015).

However, an alternative hypothesis for these $\Delta^{56}Fe_{pFe\text{-}dFe}$ patterns is based on unique reactivity timescales for individual dFe and pFe species (Fitzsimmons et al. 2017). dFe is a complex mixture of physicochemical species, particularly in regions experiencing externally supplied Fe (e.g., from dust, hydrothermal sources, or sediments) where inorganic Fe nanoparticles are found (Fitzsimmons et al. 2015). Each of these dFe species might carry a different $\delta^{56}Fe$ and might react over different timescales in ways that can be perceived as apparent $\delta^{56}Fe$ fractionation during scavenging. For instance, in a mathematical model, different dFe species (e.g., inorganic oxyhydroxides versus organically bound dFe) in a hydrothermal plume were allowed to be scavenged onto marine particles at different rates (Fitzsimmons et al. 2017). This changed the dissolved $\delta^{56}Fe$ over time without necessitating classical kinetic isotope fractionation during scavenging; indeed, it was not a certain mass of Fe that was reacting faster but a certain species of Fe that carried a unique $\delta^{56}Fe$. However, the apparent $\Delta^{56}Fe_{pFe\text{-}dFe}$ of this scavenging is entirely dependent on the original mixture and $\delta^{56}Fe$ of dFe species and the pFe scavenging regime; thus, this scavenging $\Delta^{56}Fe_{pFe\text{-}dFe}$ cannot be universally applied.

In summary, due to the complexities of the molecular mechanism of Fe scavenging in seawater, it is difficult to assign a $\Delta^{56}Fe$ to scavenging under natural conditions. However, these discussions highlight the utility of $\delta^{56}Fe$ measurements across different operational size fractions of Fe in order to access different pools of Fe species. This has been well explored in rivers (Escoube et al. 2009, 2015; Ilina et al. 2013; Mulholland et al. 2015) but less well studied in seawater (Fitzsimmons et al. 2015, Zhang et al. 2021).

6. CONCLUSIONS

Fe isotopic analyses of seawater have been performed only in the last 15 years, but the more than 3,000 analyses during that time have transformed our ability to diagnose the sources of Fe to the ocean. We have learned that end-member $\delta^{56}Fe$ signatures exist, but they must be regionally assigned, as different source regions host a variety of isotope-fractionating reactions that can drive $\delta^{56}Fe$ to variable end-member signatures, even for the same type of Fe source. This has expanded our knowledge not only of the ocean but also of the individual Fe transformations occurring in these end-member systems. The explosion of $\delta^{56}Fe$ analyses in seawater hosted by the

GEOTRACES program has revealed that by modeling Fe isotope distributions, we are able to distinguish reductive and nonreductive benthic Fe fluxes to the ocean, identify anthropogenic and natural dust fluxes, and determine which dFe species persist in hydrothermal plumes. Indeed, NRD in sediments and new insights into hydrothermal Fe speciation would not have been discovered without δ^{56}Fe. δ^{56}Fe measurements have undoubtedly provided a new dimension of Fe source partitioning, as they have been applied in nearly every global ocean basin and have been used to ground-truth source fluxes in Fe biogeochemical models.

The greatest uncertainty in the interpretation of δ^{56}Fe is the potential δ^{56}Fe fractionation during internal Fe cycling, such as biological uptake and regeneration, ligand exchange, photochemical processes, and scavenging. Realistic experimental constraints of this fractionation remain a challenge, but we have begun to infer relevant isotope effects of biological uptake and scavenging from process studies. Future δ^{56}Fe modeling efforts will combine the power of Fe concentrations and δ^{56}Fe, which should double the predictive power of this elusive but ever-critical micronutrient.

FUTURE ISSUES

1. How should we predict regionally applicable δ^{56}Fe end members? Such prediction will require not only measuring end members that have not been previously constrained (e.g., biomass burning versus wildfire Fe) but also experimentally investigating fractionation as those Fe sources meet seawater (e.g., dust solubilization by natural Fe ligands and redox fractionation at the sediment–water interface).
2. What new techniques can we use to assess the δ^{56}Fe of different fractions of the dissolved Fe pool?
3. What is the δ^{56}Fe fractionation during binding of Fe by natural organic ligands, and how does it vary with ligand type?
4. What is the δ^{56}Fe fractionation of biological Fe uptake into different phytoplankton species that utilize different Fe uptake mechanisms, based on culture? What is the δ^{56}Fe fractionation of grazing and bacterial respiration?
5. Are there δ^{56}Fe isotope effects associated with surface photochemistry?
6. What, if any, is the δ^{56}Fe fractionation associated with different mechanisms of marine dissolved Fe scavenging? When scavenging is accounted for, are δ^{56}Fe signatures faithfully transported along water masses?
7. What are the magnitude and direction of the δ^{56}Fe fractionation factor for dissolved Fe across marine oxyclines, and which processes (equilibrium, kinetic, or ligand binding) drive this?
8. How should all of these biotic and abiotic processes be parameterized in δ^{56}Fe models, and do these models provide additional insight into marine Fe biogeochemistry?

DISCLOSURE STATEMENT

J.N.F. has received funding from The Metals Company to study the effects of deep-sea mining on the marine trace metal cycles. The terms of this arrangement have been approved by Texas A&M University.

ACKNOWLEDGMENTS

We thank Janelle Steffen for compiling some of the literature δ^{56}Fe cited in this review; Matthias Sieber, Hannah Hunt, and Brent Summers for sharing unpublished data for inclusion in **Figure 1**; Fitzsimmons and Conway laboratory members and one anonymous reviewer for providing reviews of an early draft of this article; and Reiner Schlitzer for producing **Figure 1**. This work was supported by grants from the National Science Foundation to J.N.F. (OCE-1737167, OCE-1851078, OCE-1941308, OCE-2049241, and OCE-2123333) and T.M.C. (OCE-1829643, OCE-1737136, OCE-2123354, and OCE-2049214).

LITERATURE CITED

Abadie C, Lacan F, Radic A, Pradoux C, Poitrasson F. 2017. Iron isotopes reveal distinct dissolved iron sources and pathways in the intermediate versus deep Southern Ocean. *PNAS* 114:858–63

Akerman A, Poitrasson F, Oliva P, Audry S, Prunier J, Braun J-J. 2014. The isotopic fingerprint of Fe cycling in an equatorial soil–plant–water system: the Nsimi watershed, South Cameroon. *Chem. Geol.* 385:104–16

Anderson RF. 2020. GEOTRACES: accelerating research on the marine biogeochemical cycles of trace elements and their isotopes. *Annu. Rev. Mar. Sci.* 12:49–85

Anderson RF, Mawji E, Cutter GA, Measures CI, Jeandel C. 2014. GEOTRACES: changing the way we explore ocean chemistry. *Oceanography* 27(1):50–61

Beard BL, Handler RM, Scherer MM, Wu L, Czaja AD, et al. 2010. Iron isotope fractionation between aqueous ferrous iron and goethite. *Earth Planet. Sci. Lett.* 295:241–50

Beard BL, Johnson CM. 1999. High precision iron isotope measurements of terrestrial and lunar materials. *Geochim. Cosmochim. Acta* 63:1653–60

Beard BL, Johnson CM, Cox L, Sun H, Nealson KH, Aguilar C. 1999. Iron isotope biosignatures. *Science* 285:1889–92

Beard BL, Johnson CM, Von Damm KL, Poulson RL. 2003. Iron isotope constraints on Fe cycling and mass balance in oxygenated Earth oceans. *Geology* 31:629–32

Bennett SA, Rouxel O, Schmidt K, Garbe-Schonberg D, Statham PJ, German CR. 2009. Iron isotope fractionation in a buoyant hydrothermal plume, 5°S Mid-Atlantic Ridge. *Geochim. Cosmochim. Acta* 73:5619–34

Bergquist BA, Boyle EA. 2006a. Dissolved iron in the tropical and subtropical Atlantic Ocean. *Glob. Biogeochem. Cycles* 20:14

Bergquist BA, Boyle EA. 2006b. Iron isotopes in the Amazon River system: weathering and transport signatures. *Earth Planet. Sci. Lett.* 248:54–68

Boyle EA, Edmond JM, Sholkovitz ER. 1977. The mechanism of iron removal in estuaries. *Geochim. Cosmochim. Acta* 41:1313–24

Boyle EA, John S, Abouchami W, Adkins JF, Echegoyen-Sanz Y, et al. 2012. GEOTRACES IC1 (BATS) contamination-prone trace element isotopes Cd, Fe, Pb, Zn, Cu, and Mo intercalibration. *Limnol. Oceanogr. Methods* 10:653–65

Bullen TD, White AF, Childs CW, Vivit DV, Schulz MS. 2001. Demonstration of significant abiotic iron isotope fractionation in nature. *Geology* 29:699–702

Butler IB, Archer C, Vance D, Oldroyd A, Rickard D. 2005. Fe isotope fractionation on FeS formation in ambient aqueous solution. *Earth Planet. Sci. Lett.* 236:430–42

Charette MA, Kipp LE, Jensen LT, Dabrowski JS, Whitmore LM, et al. 2020. The Transpolar Drift as a source of riverine and shelf-derived trace elements to the central Arctic Ocean. *J. Geophys. Res. Oceans* 125:e2019JC015920

Chen J-B, Busigny V, Gaillardet J, Louvat P, Wang Y-N. 2014. Iron isotopes in the Seine River (France): natural versus anthropogenic sources. *Geochim. Cosmochim. Acta* 128:128–43

Chever F, Rouxel OJ, Croot PL, Ponzevera E, Wuttig K, Auro M. 2015. Total dissolvable and dissolved iron isotopes in the water column of the Peru upwelling regime. *Geochim. Cosmochim. Acta* 162:66–82

Chu NC, Johnson CM, Beard BL, German CR, Nesbitt RW, et al. 2006. Evidence for hydrothermal venting in Fe isotope compositions of the deep Pacific Ocean through time. *Earth Planet. Sci. Lett.* 245:202–17

Conway TM, Hamilton DS, Shelley RU, Aguilar-Islas AM, Landing WM, et al. 2019. Tracing and constraining anthropogenic aerosol iron fluxes to the North Atlantic Ocean using iron isotopes. *Nat. Commun.* 10:2628
Conway TM, Horner TJ, Plancherel Y, González AG. 2021. A decade of progress in understanding cycles of trace elements and their isotopes in the oceans. *Chem. Geol.* 580:120381
Conway TM, John SG. 2014. Quantification of dissolved iron sources to the North Atlantic Ocean. *Nature* 511:212–15
Conway TM, John SG. 2015. The cycling of iron, zinc and cadmium in the North East Pacific Ocean – insights from stable isotopes. *Geochim. Cosmochim. Acta* 164:262–83
Conway TM, John SG, Lacan F. 2016. Intercomparison of dissolved iron isotope profiles from re-occupation of three GEOTRACES stations in the Atlantic Ocean. *Mar. Chem.* 183:50–61
Conway TM, Rosenberg AD, Adkins JF, John SG. 2013. A new method for precise determination of iron, zinc, and cadmium stable isotope ratios in seawater by double-spike mass spectrometry. *Anal. Chim. Acta* 793:44–52
Crosby HA, Johnson CM, Roden EE, Beard BL. 2005. Coupled Fe(II)-Fe(III) electron and atom exchange as a mechanism for Fe isotope fractionation during dissimilatory iron oxide reduction. *Environ. Sci. Technol.* 39:6698–704
Crosby HA, Roden EE, Johnson CM, Beard BL. 2007. The mechanisms of iron isotope fractionation produced during dissimilatory Fe(III) reduction by *Shewanella putrefaciens* and *Geobacter sulfurreducens*. *Geobiology* 5:169–89
Dale AW, Nickelsen L, Scholz F, Hensen C, Oschlies A, Wallmann K. 2015. A revised global estimate of dissolved iron fluxes from marine sediments. *Glob. Biogeochem. Cycles* 29:691–707
Dauphas N, John SG, Rouxel O. 2017. Iron isotope systematics. *Rev. Mineral. Geochem.* 82:415–510
de Jong J, Schoemann V, Tison JL, Becquevort S, Masson F, et al. 2007. Precise measurement of Fe isotopes in marine samples by multi-collector inductively coupled plasma mass spectrometry (MC-ICP-MS). *Anal. Chim. Acta* 589:105–19
Dideriksen K, Baker JA, Stipp SLS. 2008. Equilibrium Fe isotope fractionation between inorganic aqueous Fe(III) and the siderophore complex, Fe(III)-desferrioxamine B. *Earth Planet. Sci. Lett.* 269:280–90
Dunlea AG, Tegler LA, Peucker-Ehrenbrink B, Anbar AD, Romaniello SJ, Horner TJ. 2021. Pelagic clays as archives of marine iron isotope chemistry. *Chem. Geol.* 575:120201
Ellwood MJ, Hutchins DA, Lohan MC, Milne A, Nasemann P, et al. 2015. Iron stable isotopes track pelagic iron cycling during a subtropical phytoplankton bloom. *PNAS* 112:E15–20
Ellwood MJ, Strzepek RF, Strutton PG, Trull TW, Fourquez M, Boyd PW. 2020. Distinct iron cycling in a Southern Ocean eddy. *Nat. Commun.* 11:825
Elrod VA, Berelson WM, Coale KH, Johnson KS. 2004. The flux of iron from continental shelf sediments: a missing source for global budgets. *Geophys. Res. Lett.* 31:L12307
Escoube R, Rouxel OJ, Pokrovsky OS, Schroth A, Holmes RM, Donard OF. 2015. Iron isotope systematics in Arctic rivers. *C. R. Geosci.* 347:377–85
Escoube R, Rouxel OJ, Sholkovitz E, Donard OFX. 2009. Iron isotope systematics in estuaries: the case of North River, Massachusetts (USA). *Geochim. Cosmochim. Acta* 73:4045–59
Fantle MS, DePaolo DJ. 2004. Iron isotopic fractionation during continental weathering. *Earth Planet. Sci. Lett.* 228:547–62
Fitzsimmons JN, Boyle EA. 2014. Assessment and comparison of Anopore and cross flow filtration methods for the determination of dissolved iron size fractionation into soluble and colloidal phases in seawater. *Limnol. Oceanogr. Methods* 12:244–61
Fitzsimmons JN, Carrasco GG, Wu J, Roshan S, Hatta M, et al. 2015. Partitioning of dissolved iron and iron isotopes into soluble and colloidal phases along the GA03 GEOTRACES North Atlantic Transect. *Deep-Sea Res. II* 116:130–51
Fitzsimmons JN, Conway TM, Lee J-M, Kayser R, Thyng KM, et al. 2016. Dissolved iron and iron isotopes in the southeastern Pacific Ocean. *Glob. Biogeochem. Cycles* 30:1372–95
Fitzsimmons JN, Jenkins WJ, Boyle EA. 2014. Distal transport of dissolved hydrothermal iron in the deep South Pacific Ocean. *PNAS* 111:16654–61
Fitzsimmons JN, John SG, Marsay CM, Hoffman CL, Nicholas SL, et al. 2017. Iron persistence in a distal hydrothermal plume supported by dissolved–particulate exchange. *Nat. Geosci.* 10:195

Frierdich AJ, Beard BL, Reddy TR, Scherer MM, Johnson CM. 2014. Iron isotope fractionation between aqueous Fe(II) and goethite revisited: new insights based on a multi-direction approach to equilibrium and isotopic exchange rate modification. *Geochim. Cosmochim. Acta* 139:383–98

Froelich PN, Klinkhammer G, Bender ML, Luedtke N, Heath GR, et al. 1979. Early oxidation of organic matter in pelagic sediments of the eastern equatorial Atlantic: suboxic diagenesis. *Geochim. Cosmochim. Acta* 43:1075–90

Gartman A, Findlay AJ, Luther GW III. 2014. Nanoparticulate pyrite and other nanoparticles are a widespread component of hydrothermal vent black smoker emissions. *Chem. Geol.* 366:32–41

GEOTRACES Group. 2006. *GEOTRACES Science Plan*. Baltimore, MD: Sci. Comm. Ocean. Res.

GEOTRACES Int. Data Prod. Group. 2021. *The GEOTRACES Intermediate Data Product 2021 (IDP2021)*. Data Set, Br. Oceanogr. Data Cent., Liverpool, UK. **https://doi.org/10.5285/cf2d9ba9-d51d-3b7c-e053-8486abc0f5fd**

German CR, Seyfried WE. 2014. Hydrothermal processes. In *Treatise on Geochemistry*, ed. HD Holland, KK Turekian, pp. 191–233. Oxford, UK: Elsevier. 2nd ed.

Gledhill M, Buck KN. 2012. The organic complexation of iron in the marine environment: a review. *Front. Microbiol.* 3:69

Gong Y, Xia Y, Huang F, Yu H. 2017. Average iron isotopic compositions of the upper continental crust: constrained by loess from the Chinese Loess Plateau. *Acta Geochim.* 36:125–31

Hamilton DS, Perron MMG, Bond TC, Bowie AR, Buchholz RR, et al. 2022. Earth, wind, fire, and pollution: aerosol nutrient sources and impacts on ocean biogeochemistry. *Annu. Rev. Mar. Sci.* 14:303–30

Han G, Yang K, Zeng J, Zhao Y. 2021. Dissolved iron and isotopic geochemical characteristics in a typical tropical river across the floodplain: the potential environmental implication. *Environ. Res.* 200:111452

Hayes CT, Fitzsimmons JN, Boyle EA, McGee D, Anderson RF, et al. 2015. Thorium isotopes tracing the iron cycle at the Hawaii Ocean Time-series station ALOHA. *Geochim. Cosmochim. Acta* 169:1–16

Henkel S, Kasten S, Hartmann JF, Silva-Busso A, Staubwasser M. 2018. Iron cycling and stable Fe isotope fractionation in Antarctic shelf sediments, King George Island. *Geochim. Cosmochim. Acta* 237:320–38

Henkel S, Kasten S, Poulton SW, Staubwasser M. 2016. Determination of the stable iron isotopic composition of sequentially leached iron phases in marine sediments. *Chem. Geol.* 421:93–102

Hirst C, Andersson PS, Kooijman E, Schmitt M, Kutscher L, et al. 2020. Iron isotopes reveal the sources of Fe-bearing particles and colloids in the Lena River basin. *Geochim. Cosmochim. Acta* 269:678–92

Homoky WB, Conway TM, John SG, König D, Deng F, et al. 2021. Iron colloids dominate sedimentary supply to the ocean interior. *PNAS* 118:e2016078118

Homoky WB, Hembury DJ, Hepburn LE, Mills RA, Statham PJ, et al. 2011. Iron and manganese diagenesis in deep sea volcanogenic sediments and the origins of pore water colloids. *Geochim. Cosmochim. Acta* 75:5032–48

Homoky WB, John SG, Conway TM, Mills RA. 2013. Distinct iron isotopic signatures and supply from marine sediment dissolution. *Nat. Commun.* 4:2143

Homoky WB, Severmann S, Mills RA, Statham PJ, Fones GR. 2009. Pore-fluid Fe isotopes reflect the extent of benthic Fe redox recycling: evidence from continental shelf and deep-sea sediments. *Geology* 37:751–54

Horner TJ, Little S, Conway T, Farmer J, Hertzberg JE, et al. 2021. Bioactive trace metals and their isotopes as paleoproductivity proxies: an assessment using GEOTRACES-era data. *Glob. Biogeochem. Cycles* 35:e2020GB006814

Horner TJ, Williams HM, Hein JR, Saito MA, Burton KW, et al. 2015. Persistence of deeply sourced iron in the Pacific Ocean. *PNAS* 112:1292–97

Hutchins DA, Witter AE, Butler A, Luther GW III. 1999. Competition among marine phytoplankton for different chelated iron species. *Nature* 400:858–61

Icopini GA, Anbar AD, Ruebush SS, Tien M, Brantley SL. 2004. Iron isotope fractionation during microbial reduction of iron: the importance of adsorption. *Geology* 32:205–8

Ilina SM, Poitrasson F, Lapitskiy SA, Alekhin YV, Viers J, Pokrovsky OS. 2013. Extreme iron isotope fractionation between colloids and particles of boreal and temperate organic-rich waters. *Geochim. Cosmochim. Acta* 101:96–111

Ingri J, Malinovsky D, Rodushkin I, Baxter DC, Widerlund A, et al. 2006. Iron isotope fractionation in river colloidal matter. *Earth Planet. Sci. Lett.* 245:792–98

Jickells TD, An ZS, Andersen KK, Baker AR, Bergametti G, et al. 2005. Global iron connections between desert dust, ocean biogeochemistry, and climate. *Science* 308:67–71

John SG, Adkins J. 2012. The vertical distribution of iron stable isotopes in the North Atlantic near Bermuda. *Glob. Biogeochem. Cycles* 26:GB2034

John SG, Adkins JF. 2010. Analysis of dissolved iron isotopes in seawater. *Mar. Chem.* 119:65–76

John SG, Geis RW, Saito MA, Boyle EA. 2007. Zinc isotope fractionation during high-affinity and low-affinity zinc transport by the marine diatom *Thalassiosira oceanica*. *Limnol. Oceanogr.* 52:2710–14

John SG, Helgoe J, Townsend E, Weber T, DeVries T, et al. 2018. Biogeochemical cycling of Fe and Fe stable isotopes in the Eastern Tropical South Pacific. *Mar. Chem.* 201:66–76

John SG, King A, Hutchins D, Adkins J, Fu F, et al. 2012a. *Biological, chemical, electrochemical, and photochemical fractionation of Fe isotopes*. Paper presented at the American Geophysical Union Fall Meeting, San Francisco, CA, Dec. 3–7

John SG, Mendez J, Moffett J, Adkins J. 2012b. The flux of iron and iron isotopes from San Pedro Basin sediments. *Geochim. Cosmochim. Acta* 93:14–29

Johnson CM, Beard B, Weyer S. 2020. *Iron Geochemistry: An Isotopic Perspective*. Cham, Switz.: Springer

Johnson CM, Roden EE, Welch SA, Beard BL. 2005. Experimental constraints on Fe isotope fractionation during magnetite and Fe carbonate formation coupled to dissimilatory hydrous ferric oxide reduction. *Geochim. Cosmochim. Acta* 69:963–93

Klar JK, Homoky WB, Statham PJ, Birchill AJ, Harris EL, et al. 2017a. Stability of dissolved and soluble Fe(II) in shelf sediment pore waters and release to an oxic water column. *Biogeochemistry* 135:49–67

Klar JK, James RH, Gibbs D, Lough A, Parkinson I, et al. 2017b. Isotopic signature of dissolved iron delivered to the Southern Ocean from hydrothermal vents in the East Scotia Sea. *Geology* 45:351–54

Klar JK, Schlosser C, Milton JA, Woodward E, Lacan F, et al. 2018. Sources of dissolved iron to oxygen minimum zone waters on the Senegalese continental margin in the tropical North Atlantic Ocean: insights from iron isotopes. *Geochim. Cosmochim. Acta* 236:60–78

König D, Conway T, Ellwood M, Homoky W, Tagliabue A. 2021. Constraints on the cycling of iron isotopes from a global ocean model. *Glob. Biogeochem. Cycles* 35:e2021GB006968

Kurisu M, Adachi K, Sakata K, Takahashi Y. 2019. Stable isotope ratios of combustion iron produced by evaporation in a steel plant. *ACS Earth Space Chem.* 3:588–98

Kurisu M, Sakata K, Miyamoto C, Takaku Y, Iizuka T, Takahashi Y. 2016a. Variation of iron isotope ratios in anthropogenic materials emitted through combustion processes. *Chem. Lett.* 45:970–72

Kurisu M, Sakata K, Uematsu M, Ito A, Takahashi Y. 2021. Contribution of combustion Fe in marine aerosols over the northwestern Pacific estimated by Fe stable isotope ratios. *Atmos. Chem. Phys.* 21:16027–50

Kurisu M, Takahashi Y, Iizuka T, Uematsu M. 2016b. Very low isotope ratio of iron in fine aerosols related to its contribution to the surface ocean. *J. Geophys. Res. Atmos.* 121:11119–36

Labatut M, Lacan F, Pradoux C, Chmeleff J, Radic A, et al. 2014. Iron sources and dissolved-particulate interactions in the seawater of the Western Equatorial Pacific, iron isotope perspectives. *Glob. Biogeochem. Cycles* 28:1044–65

Lacan F, Francois R, Ji Y, Sherrell RM. 2006. Cadmium isotopic composition in the ocean. *Geochim. Cosmochim. Acta* 70:5104–18

Lacan F, Radic A, Jeandel C, Poitrasson F, Sarthou G, et al. 2008. Measurement of the isotopic composition of dissolved iron in the open ocean. *Geophys. Res. Lett.* 35:L24610

Lannuzel D, Vancoppenolle M, Van der Merwe P, De Jong J, Meiners KM, et al. 2016. Iron in sea ice: review and new insights. *Elem. Sci. Anthr.* 4:000130

Levasseur S, Frank M, Hein J, Halliday AN. 2004. The global variation in the iron isotope composition of marine hydrogenetic ferromanganese deposits: implications for seawater chemistry? *Earth Planet. Sci. Lett.* 224:91–105

Liu X, Millero FJ. 2002. The solubility of iron in seawater. *Mar. Chem.* 77:43–54

Lough AJM, Klar JK, Homoky WB, Comer-Warner SA, Milton JA, et al. 2017. Opposing authigenic controls on the isotopic signature of dissolved iron in hydrothermal plumes. *Geochim. Cosmochim. Acta* 202:1–20

Majestic BJ, Anbar AD, Herckes P. 2009. Elemental and iron isotopic composition of aerosols collected in a parking structure. *Sci. Total Environ.* 407:5104–9

Marcus MA, Edwards KJ, Gueguen B, Fakra SC, Horn G, et al. 2015. Iron mineral structure, reactivity, and isotopic composition in a South Pacific Gyre ferromanganese nodule over 4 Ma. *Geochim. Cosmochim. Acta* 171:61–79

Marsay CM, Aguilar-Islas A, Fitzsimmons JN, Hatta M, Jensen LT, et al. 2018a. Dissolved and particulate trace elements in late summer Arctic melt ponds. *Mar. Chem.* 204:70–85

Marsay CM, Lam PJ, Heller MI, Lee J-M, John SG. 2018b. Distribution and isotopic signature of ligand-leachable particulate iron along the GEOTRACES GP16 East Pacific Zonal Transect. *Mar. Chem.* 201:198–211

Martin JH. 1990. Glacial-interglacial CO_2 change: the iron hypothesis. *Paleoceanography* 5:1–13

Mead C, Herckes P, Majestic BJ, Anbar AD. 2013. Source apportionment of aerosol iron in the marine environment using iron isotope analysis. *Geophys. Res. Lett.* 40:5722–27

Moore JK, Doney SC, Glover DM, Fung IY. 2002. Iron cycling and nutrient-limitation patterns in surface waters of the world ocean. *Deep-Sea Res. II* 49:463–507

Morel FMM, Kustka AB, Shaked Y. 2008. The role of unchelated Fe in the iron nutrition of phytoplankton. *Limnol. Oceanogr.* 53:400–4

Morgan JLL, Wasylenki LE, Nuester J, Anbar AD. 2010. Fe isotope fractionation during equilibration of Fe-organic complexes. *Environ. Sci. Technol.* 44:6095–101

Mulholland DS, Flament P, de Jong J, Mattielli N, Deboudt K, et al. 2021. In-cloud processing as a possible source of isotopically light iron from anthropogenic aerosols: new insights from a laboratory study. *Atmos. Environ.* 259:118505

Mulholland DS, Poitrasson F, Boaventura GR, Allard T, Vieira LC, et al. 2015. Insights into iron sources and pathways in the Amazon River provided by isotopic and spectroscopic studies. *Geochim. Cosmochim. Acta* 150:142–59

Nasemann P, Gault-Ringold M, Stirling CH, Koschinsky A, Sander SG. 2018. Processes affecting the isotopic composition of dissolved iron in hydrothermal plumes: a case study from the Vanuatu back-arc. *Chem. Geol.* 476:70–84

Nier AO. 1939. The isotopic constitution of iron and chromium. *Phys. Rev.* 55:1143

Owens JD, Lyons TW, Li X, Macleod KG, Gordon G, et al. 2012. Iron isotope and trace metal records of iron cycling in the proto-North Atlantic during the Cenomanian-Turonian oceanic anoxic event (OAE-2). *Paleoceanography* 27:PA3223

Perron MMG, Meyerink S, Corkill M, Strzelec M, Proemse BC, et al. 2022. Trace elements and nutrients in wildfire plumes to the southeast of Australia. *Atmos. Res.* 270:106084

Pinedo-González P, Hawco NJ, Bundy RM, Armbrust EV, Follows MJ, et al. 2020. Anthropogenic Asian aerosols provide Fe to the north Pacific Ocean. *PNAS* 117:27862–68

Poitrasson F, Cruz Vieira L, Seyler P, dos Santos Pinheiro GM, Santos Mulholland D, et al. 2014. Iron isotope composition of the bulk waters and sediments from the Amazon River Basin. *Chem. Geol.* 377:1–11

Radic A, Lacan F, Murray JW. 2011. Iron isotopes in the seawater of the equatorial Pacific Ocean: new constraints for the oceanic iron cycle. *Earth Planet. Sci. Lett.* 306:1–10

Raiswell R, Tranter M, Benning LG, Siegert M, De'ath R, et al. 2006. Contributions from glacially derived sediment to the global iron (oxyhydr)oxide cycle: implications for iron delivery to the oceans. *Geochim. Cosmochim. Acta* 70:2765–80

Resing JA, Sedwick PN, German CR, Jenkins WJ, Moffett JW, et al. 2015. Basin-scale transport of hydrothermal dissolved metals across the South Pacific Ocean. *Nature* 523:200–6

Revels BN, Ohnemus DC, Lam PJ, Conway TM, John SG. 2015a. The isotopic signature and distribution of particulate iron in the North Atlantic Ocean. *Deep-Sea Res. II* 116:321–31

Revels BN, Zhang R, Adkins JF, John SG. 2015b. Fractionation of iron isotopes during leaching of natural particles by acidic and circumneutral leaches and development of an optimal leach for marine particulate iron isotopes. *Geochim. Cosmochim. Acta* 166:92–104

Rolison JM, Stirling CH, Middag R, Gault-Ringold M, George E, Rijkenberg MJ. 2018. Iron isotope fractionation during pyrite formation in a sulfidic Precambrian ocean analogue. *Earth Planet. Sci. Lett.* 488:1–13

Rouxel O, Auro M. 2010. Iron isotope variations in coastal seawater determined by multicollector ICP-MS. *Geostand. Geoanal. Res.* 34:135–44

Rouxel O, Dobbek N, Ludden J, Fouquet Y. 2003. Iron isotope fractionation during oceanic crust alteration. *Chem. Geol.* 202:155–82

Rouxel O, Shanks WC III, Bach W, Edwards KJ. 2008a. Integrated Fe- and S-isotope study of seafloor hydrothermal vents at East Pacific Rise 9–10°N. *Chem. Geol.* 252:214–27

Rouxel O, Sholkovitz E, Charette M, Edwards KJ. 2008b. Iron isotope fractionation in subterranean estuaries. *Geochim. Cosmochim. Acta* 72:3413–30

Rouxel O, Toner BM, Germain Y, Glazer B. 2018. Geochemical and iron isotopic insights into hydrothermal iron oxyhydroxide deposit formation at Loihi Seamount. *Geochim. Cosmochim. Acta* 220:449–82

Rouxel O, Toner BM, Manganini SJ, German CR. 2016. Geochemistry and iron isotope systematics of hydrothermal plume fall-out at East Pacific Rise 9°50′N. *Chem. Geol.* 441:212–34

Roy M, Rouxel O, Martin JB, Cable JE. 2012. Iron isotope fractionation in a sulfide-bearing subterranean estuary and its potential influence on oceanic Fe isotope flux. *Chem. Geol.* 300–301:133–42

Rudge JF, Reynolds BC, Bourdon B. 2009. The double spike toolbox. *Chem. Geol.* 265:420–31

Rudnick RL, Gao S. 2014. Composition of the continental crust. In *Treatise on Geochemistry*, ed. HD Holland, KK Turekian, pp. 1–51. Oxford, UK: Elsevier. 2nd ed.

Sander SG, Koschinsky A. 2011. Metal flux from hydrothermal vents increased by organic complexation. *Nat. Geosci.* 4:145–50

Schlitzer R, Anderson RF, Dodas EM, Lohan M, Geibert W, et al. 2018. The GEOTRACES Intermediate Data Product 2017. *Chem. Geol.* 493:210–23

Scholz F, Severmann S, McManus J, Noffke A, Lomnitz U, Hensen C. 2014. On the isotope composition of reactive iron in marine sediments: redox shuttle versus early diagenesis. *Chem. Geol.* 389:48–59

Schroth AW, Crusius J, Chever F, Bostick BC, Rouxel OJ. 2011. Glacial influence on the geochemistry of riverine iron fluxes to the Gulf of Alaska and effects of deglaciation. *Geophys. Res. Lett.* 38:L16605

Severmann S, Johnson CM, Beard BL, German CR, Edmonds HN, et al. 2004. The effect of plume processes on the Fe isotope composition of hydrothermally derived Fe in the deep ocean as inferred from the Rainbow vent site, Mid-Atlantic Ridge, 36°14′N. *Earth Planet. Sci. Lett.* 225:63–76

Severmann S, Johnson CM, Beard BL, McManus J. 2006. The effect of early diagenesis on the Fe isotope compositions of porewaters and authigenic minerals in continental margin sediments. *Geochim. Cosmochim. Acta* 70:2006–22

Severmann S, McManus J, Berelson WM, Hammond DE. 2010. The continental shelf benthic iron flux and its isotope composition. *Geochim. Cosmochim. Acta* 74:3984–4004

Sharma M, Polizzotto M, Anbar AD. 2001. Iron isotopes in hot springs along the Juan de Fuca Ridge. *Earth Planet. Sci. Lett.* 194:39–51

Sieber M, Conway TM, de Souza G, Hassler CS, Ellwood MJ, Vance D. 2021. Isotopic fingerprinting of biogeochemical processes and iron sources in the iron-limited surface Southern Ocean. *Earth Planet. Sci. Lett.* 567:116967

Skulan JL, Beard BL, Johnson CM. 2002. Kinetic and equilibrium Fe isotope fractionation between aqueous Fe(III) and hematite. *Geochim. Cosmochim. Acta* 66:2995–3015

Staubwasser M, Schoenberg R, von Blanckenburg F, Krüger S, Pohl C. 2013. Isotope fractionation between dissolved and suspended particulate Fe in the oxic and anoxic water column of the Baltic Sea. *Biogeosciences* 10:233–45

Stevenson E, Fantle M, Das S, Williams H, Aciego S. 2017. The iron isotopic composition of subglacial streams draining the Greenland ice sheet. *Geochim. Cosmochim. Acta* 213:237–54

Tagliabue A, Aumont O, DeAth R, Dunne JP, Dutkiewicz S, et al. 2016. How well do global ocean biogeochemistry models simulate dissolved iron distributions? *Glob. Biogeochem. Cycles* 30:149–74

Tagliabue A, Bopp L, Dutay J-C, Bowie AR, Chever F, et al. 2010. Hydrothermal contribution to the oceanic dissolved iron inventory. *Nat. Geosci.* 3:252–56

Tagliabue A, Bowie AR, Boyd PW, Buck KN, Johnson KS, Saito MA. 2017. The integral role of iron in ocean biogeochemistry. *Nature* 543:51–59

Teng F-Z, Dauphas N, Huang S, Marty B. 2013. Iron isotopic systematics of oceanic basalts. *Geochim. Cosmochim. Acta* 107:12–26

Teutsch N, von Gunten U, Porcelli D, Cirpka OA, Halliday AN. 2005. Adsorption as a cause for iron isotope fractionation in reduced groundwater. *Geochim. Cosmochim. Acta* 69:4175–85

Twining BS, Baines SB. 2013. The trace metal composition of marine phytoplankton. *Annu. Rev. Mar. Sci.* 5:191–215

Valley GE, Anderson HH. 1947. A comparison of the abundance ratios of the isotopes of terrestrial and of meteoritic iron. *J. Am. Chem. Soc.* 69:1871–75

von Blanckenburg F, von Wirén N, Guelke M, Weiss DJ, Bullen TD. 2009. Fractionation of metal stable isotopes by higher plants. *Elements* 5:375–80

Waeles M, Baker AR, Jickells T, Hoogewerff J. 2007. Global dust teleconnections: aerosol iron solubility and stable isotope composition. *Environ. Chem.* 4:233–37

Wang W, Lough A, Lohan MC, Connelly DP, Cooper M, et al. 2021. Behavior of iron isotopes in hydrothermal systems: Beebe and Von Damm vent fields on the mid-Cayman ultraslow-spreading ridge. *Earth Planet. Sci. Lett.* 575:117200

Welch SA, Beard BL, Johnson CM, Braterman PS. 2003. Kinetic and equilibrium Fe isotopic fractionation between aqueous Fe(II) and Fe(III). *Geochim. Cosmochim. Acta* 67:4231–50

Wu L, Beard BL, Roden EE, Johnson CM. 2011. Stable iron isotope fractionation between aqueous Fe(II) and hydrous ferric oxide. *Environ. Sci. Technol.* 45:1847–52

Zhang R, Jensen L, Fitzsimmons J, Sherrell RM, Lam P, et al. 2021. Iron isotope biogeochemical cycling in the Western Arctic Ocean. *Glob. Biogeochem. Cycles* 35:e2021GB006977

Zhang R, John SG, Zhang J, Ren J, Wu Y, et al. 2015. Transport and reaction of iron and iron stable isotopes in glacial meltwaters on Svalbard near Kongsfjorden: from rivers to estuary to ocean. *Earth Planet. Sci. Lett.* 424:201–11

Zhu X-K, O'Nions RK, Guo Y, Reynolds BC. 2000. Secular variation of iron isotopes in North Atlantic deep water. *Science* 287:2000–2

Annual Review of Marine Science

Volume 15, 2023

Contents

Errata

An online log of corrections to *Annual Review of Marine Science* articles may be found at http://www.annualreviews.org/errata/marine